Suppression of unpolarized background interferences for Raman spectroscopy under continuous operation

Kim, Haisol; Aldén, Marcus; Brackmann, Christian

Published in:
Optics Express

DOI:
10.1364/OE.414677

2021

Document Version:
Publisher's PDF, also known as Version of record

Research Article | Vol. 29, No. 2 / 18 January 2021 / Optics Express 1048
Optics EXPRESS

Suppression of unpolarized background interferences for Raman spectroscopy under continuous operation

HAISOL KIM, MARCUS ALDÉN, AND CHRISTIAN BRACKMANN*

Division of Combustion Physics, Department of Physics, Lund University, P.O. Box 118, Lund 22100, Sweden
*Christian.Brackmann@forbrf.lth.se

Abstract: A time-resolving filtering technique developed to improve background suppression in Raman spectroscopy is presented and characterized. The technique enables separation of signal contributions via their polarization dependency by the addition of a waveplate to a normal measurement system and data post-processing. As a result, background interferences of broadband laser-induced fluorescence and incandescence, as well as flame luminosity and blackbody radiation, were effectively suppressed from Raman spectra. Experimental setting parameters of the method were investigated under well-controlled conditions to assess their impact on the background-filtering ability, and the overall trend was understood. The fluorescence background was effectively suppressed for all investigated settings of modulation period, number of accumulations, and recording duration, with the spectrum quality preserved after the filtering. For practical application, the method was tested for measurements in a sooting flame accompanied by a strong luminosity and interfering laser-induced background signals. The technique resulted in a 200-fold decrease of the background and allowed for quantitative analyses of concentrations and temperatures from the filtered data. Thus, the method shows strong potential to extend the applicability of Raman spectroscopy, in particular for *in situ* diagnostics under challenging experimental conditions.

1. Introduction

Raman spectroscopy is a powerful laser-based diagnostic technique to detect multiple chemical species simultaneously and conduct quantitative analyses of concentrations and temperatures. The inelastic Raman scattering signals appear in a spectrum located relative to the wavelength of the excitation laser, and therefore, it is not required to tune the laser to a specific wavelength, which makes the setup of Raman spectroscopy less complicated than that of many other techniques. For these reasons, Raman spectroscopy is considered an excellent method for studies in various research fields, e.g., combustion, material science, environmental science, and planetary exploration, when it is demanded to detect many kinds of chemical species with quantitative information.

However, Raman spectroscopy has a downside that the signal is weak, which often diminishes all the advantages previously mentioned. In a quantitative comparison for gas, the intensity of Raman scattering is known to be on the order of 0.1% of the Rayleigh scattering intensity, which, in turn, is about 0.1% of the strength of a radiation source [1]. Fortunately, Raman scattering signals are shifted from the wavelength of the laser source and the elastic Rayleigh scattering, so the signals do not interfere with each other if the Raman shift for a target molecule is not too small. However, if there are sources of broadband background signals, e.g., black body radiation and fluorescence, in the measurement volume, the chance of Raman spectroscopy to be successfully employed for measurements is very small. These challenges are particularly

#414677 https://doi.org/10.1364/OE.414677
Journal © 2021 Received 10 Nov 2020; revised 4 Dec 2020; accepted 9 Dec 2020; published 5 Jan 2021

Optics EXPRESS

encountered when applying the method for *in situ* diagnostics in different experimental setups and even more so in studies of reactive flows, such as investigations of combustion processes.

In this study, we have developed a technique to overcome the obstacle mentioned above of utilizing Raman spectroscopy due to the unwanted background signals. It is a filtering technique that can suppress polarization-independent signals such as blackbody radiation and most fluorescence. The method is named 'polarization lock-in filtering (PLF)' and was inspired by a spatial lock-in filtering technique previously demonstrated for spectroscopic techniques called 'periodic shadowing' [2] and a polarization-separation method. The PLF technique features a novelty as it can be employed for time-resolved measurements, which was not feasible with most of the existing background suppression methods.

Since the introduction of Raman spectroscopy, there have been a variety of approaches to tackle the limitations of applying the technique. Among them, some similar approaches to this study are selected here and compared with our method. Extensive reviews of the various approaches by Wei et al. and De Luca et al. were helpful for this purpose [3,4]. According to their works, the background suppression methods could be categorized into six kinds: mathematical, polarization gating, time-domain, frequency-domain, wavelength-domain, and modulated Raman spectroscopy. The PLF technique falls into the polarization-gating methods, in accordance with their definition, and other previous works in the same category could be studied. The concept of suppressing luminescence using the polarization characteristics of Raman scattering was first presented by Arguello et al. [5]. Their work suggested a lock-in amplification concept, which resembles the current work but is not providing detailed parameters and applications of the method. While the majority of previous works in the polarization gating category presented improvements in spectral quality and the range of application, the temporal resolution was not considered or had to be compromised [6–9]. The study of Grünefeld et al. is a good example of making Raman spectroscopy possible by overcoming fluorescence interferences for measurements in a spray flame and in a realistic internal combustion engine [10]. They have shifted the laser polarization using an MgF_2 plate, and spectra acquired for the different polarization orientations were compared. However, in order to completely separate two images under different laser polarizations, very accurate control and synchronization of the polarization change and image recording is required for continuous operation. Therefore, keeping temporal information is challenging with the direct subtraction of subsequent spectra. Later, Kojima et al. have introduced a method to realize the concept more conveniently by employing a frame-transfer CCD [11]. Another work in this category, presented by Magnotti et al., introduced an approach of detecting two different polarization components of signals by employing individual detectors for each polarization component [12]. They could obtain interference-free Raman spectra in fuel-rich hydrocarbon flames, and this approach would allow for temporally resolved measurements if the setup is operated continuously. However, the dual detector setup may impose practical limitations. On the other hand, the PLF technique in this study is based on the use of a single detector and has the advantage of conserving temporal resolution while eliminating unwanted signals from the measurement volume with a similar approach to the previous works. The optical arrangement of the method is rather uncomplicated as only one additional component is added to the ordinary setup. Moreover, mathematical post-processing of the data makes acquisition conditions less limited regarding synchronization between the polarization and the recording timing.

The main goals of this study are to validate the PLF concept and present its potential to extend the applicability of Raman spectroscopy for experiments under challenging conditions. This has been achieved with measurements in ambient air, in air seeded with acetone to provide a controlled fluorescence background, and in a luminous sooty flame with background contributions from blackbody radiation and fluorescence. The effects of various experimental parameters were investigated, and the improvements in the quality of Raman spectra were examined. Some

Optics EXPRESS

discoveries from the ambient air spectra are included to provide an example of applications in other fields as well.

2. Method

2.1. Polarization Lock-In Filtering (PLF)

As previously mentioned, the PLF technique was largely inspired by the periodic shadowing (PS) technique. For both the PS and PLF methods, modulated signals are utilized to identify the contributions of targeted components and unwanted backgrounds on the recorded signal. The input data for the PS method are spectra acquired as images with the detection wavelength on the x-axis and spatial coordinate along the spectrometer slit on the y-axis. When coupled into the spectrometer, the signal is spatially modulated by a grating element installed on the slit. As a result of a Fourier filtering operation, the spatial resolution of the data is maintained after the post-processing.

The PLF technique utilizes the modulation of signal intensity with time, achieved by having the polarization of the incident laser continuously shifted between vertical and horizontal orientation. Similar to the PS method, the PLF is based on the acquisition of spectral images, but in this case, with temporal modulation registered along the y-axis. As a result, the intensity of polarization-dependent signals oscillate along the y-axis of the image, as shown in Fig. 1(a), and the final data after the filtering maintains temporally varying information like Fig. 1(d). Raman scattering signals are highly polarization-dependent and exhibit a fully toroidal radiation pattern with almost no signal emitted along the dipole axis, i.e., the axis parallel to the incident beam polarization [13]. Therefore, when the laser polarization is shifted from vertical to horizontal orientation, the radiation pattern rotates accordingly, so that a small amount of radiation is collected from the side. On the other hand, depolarized signals, e.g., fluorescence, do not vary with the laser polarization in this way, and therefore, such signals are recorded continuously without the modulation pattern.

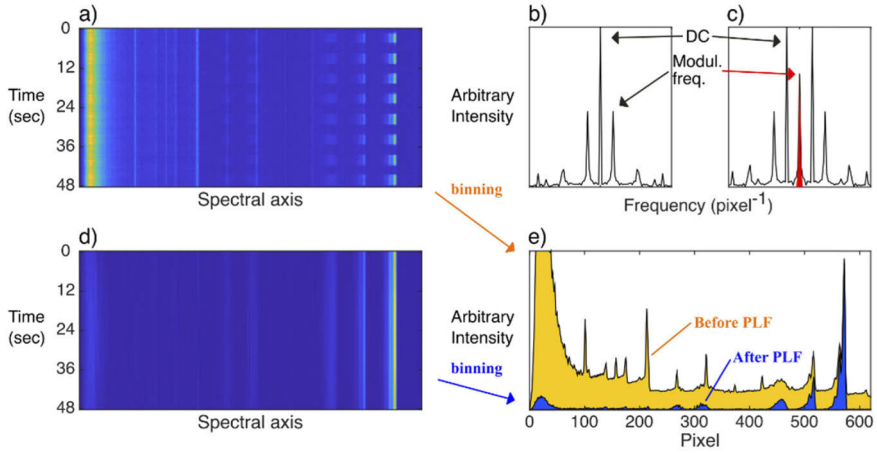

Fig. 1. Two-dimensional a) input and d) output data of the PLF technique. Panel b) shows the Fourier transform of the input data, while panel c) is the Fourier transform of the input data multiplied by a reference signal having the modulation frequency. The red region is selected by a bandpass filter. Panel e) presents intensity-averaged spectra along the image y-axis before and after applying the technique, and polarization-independent backgrounds have been effectively suppressed. The data set is taken from measurements in a sooting flame.

The basic principle of the PLF method is the same as for other polarization-separation methods, but the specialty of the technique is a continuous mode of operation that allows for measurements

Optics EXPRESS

under moderately time-varying conditions. The first step of the process is a Fourier transform of the two-dimensional data with periodicity from the modulation [Figs. 1(a) and 1(b)]. At second, a bandpass filter is applied to the transformed data, and a part of information with the periodicity is selected [Fig. 1(c)]. At last, the filtered part of the data is inversely Fourier transformed to reconstruct data where the periodicity is removed, and the temporal resolution is retrieved [Fig. 1(d)]. Theoretically, the temporal resolution after the filtering is half that of the input data before the filtering. In addition, due to the filtering process, it is not required to synchronize the modulation of the laser beam polarization and data recording timing. For more detailed procedures and a mathematical explanation of the filtering process, readers are referred to the previous study by Kristensson et al. [2].

2.2. Experimental

A schematic of the experimental setup is presented in Fig. 2, and it can be separated into a laser part, a detection part, a polarization lock-in filtering (PLF) part, and a measurement volume part. The laser part contains an Nd:YAG laser (HD40I-OE, Edgewave) operated at 532 nm with a repetition rate of 5 kHz and an average power set between 8 and 25 W depending on the objects measured. The laser beam was guided by mirrors and focused by a plano-convex lens with a focal length of 200 mm, and the focal region defined the center of the measurement volume. In order to increase the signal, an additional plano-convex lens and two mirrors were installed after the measurement volume in order to form a double-pass configuration and increase the signal by a factor of 2 (cf., Fig. 2).

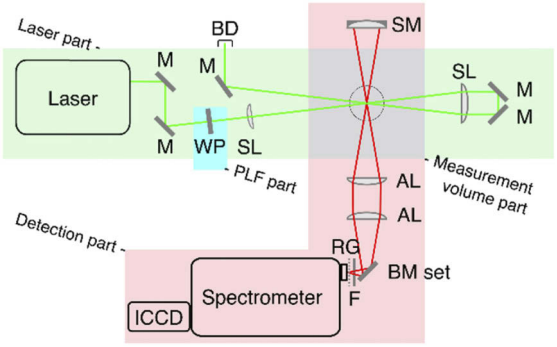

Fig. 2. Schematic of the experimental setup for Raman spectroscopy. M – mirror, WP – half-waveplate on rotation mount, SL – spherical lens, SM – spherical mirror, BD – beam dump, AL – achromatic lens, BM set – a pair of broadband mirrors for image rotation, F – 532 nm longpass filter, RG – Ronchi grating, and ICCD – intensified CCD camera.

The detection part was composed of collection lenses, mirrors, a spectrometer, and an intensified CCD camera. Two achromatic lenses with a focal length of 200 mm were placed to collect the signal, and a pair of aluminum mirrors were installed in front of the spectrometer to rotate the image of the probe volume 90 degrees so that the signal generated along the beam is guided into the vertically oriented slit. A longpass filter (532 nm EdgeBasic, Semrock) was placed in front of the slit in order to minimize background contributions by signals at the laser wavelength, e.g., elastic scattering. A concave aluminum mirror was placed on the opposite side of the measurement volume from the spectrometer to also capture signal scattered toward the other direction. Raman spectra were acquired by a Schmidt-Czerny-Turner type spectrometer (IsoPlane SCT320, Princeton Instruments) with interchangeable gratings of 600 and 1800 lines/mm, and an intensified CCD (PI-MAX 4, Princeton Instruments) connected. The ICCD recorded images in synchronization with the laser, and an on-chip-accumulation function was used to minimize

Optics EXPRESS

readout noise. The intensifier gate was set to 100 ns for the air/acetone measurements and to 40 ns for the flame measurements to reject continuous background, e.g., ceiling light and flame emission. The number of on-chip accumulations ranged from 1000-4000, which corresponds to acquisition times of 0.2-0.8 seconds.

A Ronchi grating of 5 lines/mm was installed on the entrance slit of the spectrometer in order to also utilize the PS method. The method is known to effectively suppress effects of stray light inside and outside the spectrometer and would improve the quality of spectra in this study as well [2]. Therefore, in the following, 'Raw spectra' or 'Before the PLF technique' results refer to spectra that have been processed through the PS method. After the PS process, these data were put through the PLF post-processing. The objects measured in this study were operated under steady-state conditions, so the data sets were averaged in time. The intensity of each spectrum was compensated by the wavelength-dependent sensitivity of the camera. The sensitivity along the spectral domain was obtained by utilizing a broadband intensity calibration lamp (IES 1000, Labsphere). A smoothing filter with a span of 5 pixels was applied to each spectrum in the data reduction procedure and following analyses to lower the noise level.

A half-wave plate on a motorized rotation mount (ELL14, Thorlabs) was placed in the laser beam path before the focusing lens, as shown in Fig. 2, to implement the PLF technique. An ideal modulation of the polarization for quantitative analyses requires continuous rotation of the waveplate, resulting in a sinusoidal amplitude modulation. However, due to heating of the rotation mount, an angular oscillation mode was used instead, and therefore, the modulation waveform was closer to a square wave. The modulation period, i.e., the time for changing the polarization from a vertical orientation to horizontal and back to vertical again has been varied to study the effect of this parameter, which will be discussed in section 3.2.

Three different objects were investigated. At first, Raman signals from ambient air were investigated in order to validate the PLF concept. At second, acetone vapor was seeded to an airflow by passing the flow through a reservoir with liquid acetone. The flow was released to the ambient air through a porous-plug McKenna burner to obtain a uniform distribution of the air-acetone mixture across the measurement volume. The center of the burner was positioned at the location where the beams were focused, and the height of the laser beams was set to 3 mm above the burner plug surface. A portion of the incident 532 nm beam was frequency-doubled by inserting a BBO crystal in the path before the beam reached the measurement volume. The generated 266 nm beam induced acetone fluorescence, while the residual 532 nm beam was used for Raman scattering. This arrangement enabled to introduce a well-controlled fluorescence background to the Raman spectrum and allowed to characterize the performance of the PLF method in detail. At last, a sooting ethylene/air flame stabilized on the McKenna burner, as shown in Fig. 3, was investigated. The equivalence ratio of the flame was set to Φ=2.0, where the flame showed luminous blackbody radiation from soot at equivalence ratios higher than 1.7. The height of the burner was adjustable to collect signals from various heights of the flat flame.

Fig. 3. Luminous ethylene/air flame at equivalence ratio Φ=2.0. The flame photo was taken through a 532 nm notch filter to block strong green light from the laser, and the brightness-contrast level has been adjusted to make the burner visible.

Optics EXPRESS

3. Results and discussions

3.1. Validation of the PLF technique

Raman spectroscopy with PLF was carried out on ambient air in order to validate the concept and check that the spectral information remains after the data processing. Overall, up to 90% of the already low background level has been removed, and the results are presented in Fig. 4, including spectra retrieved before processing, after PS processing, and after combined PS and PLF processing. Signal intensities were normalized to the maximum intensity of a nitrogen peak for better comparison, and it can be seen that spectral shapes are preserved without distortions.

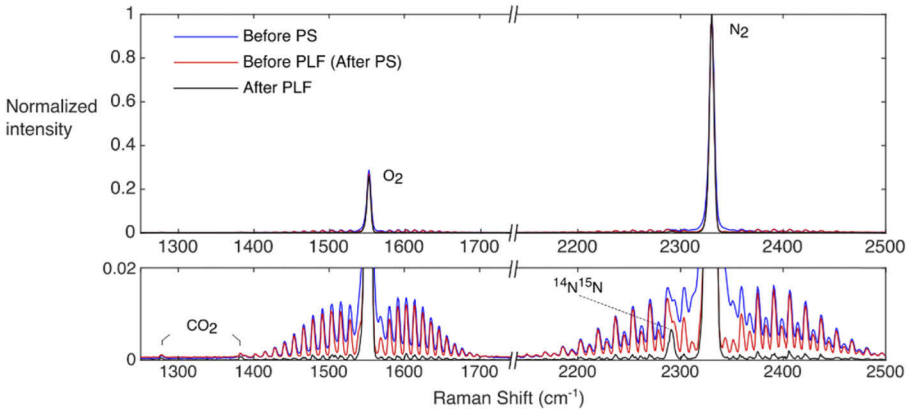

Fig. 4. Raman spectra of O_2, N_2, and CO_2 in ambient air with and without applying the PS and the PLF technique. O- and S-branches of the vibrational Raman peaks are suppressed through the filtering, and therefore, Q-branch vibrational Raman signals of CO_2 and $^{14}N^{15}N$ are clearly observed and separated from signals of O_2 and $^{14}N_2$, respectively.

Some features of the PLF technique are illustrated with this result. At first, the PLF only preserves incident-polarization-dependent signals, and therefore, ro-vibrational O- and S-branches were weakened significantly compared with Q-branch Raman signals due to their large depolarization ratios, i.e., lower polarization dependency. The depolarization ratio of the Q-branch Raman signal is a function of the Placzek-Teller coefficient and polarizability tensor, which gives 0.01 for nitrogen, while that of O- and S-branches is always 0.75 independent of the type of molecule [14]. Therefore, the O- and S-branches of oxygen and nitrogen were suppressed through the filtering process by a factor of 8, as shown in Fig. 4. As a result, the Raman scattering signals from carbon dioxide at 1280 and 1380 cm^{-1} could be well separated from the O-branch of oxygen. In addition, the Q-branch vibrational Raman signal of a rare stable nitrogen isotope, $^{14}N^{15}N$, was clearly distinguished at Raman shift 2290 cm^{-1}. The integrated signal of $^{14}N^{15}N$ was 0.7% of the area under the peak of the most abundant $^{14}N_2$ at 2331 cm^{-1}. The value is in good agreement with the known natural abundance of $^{14}N^{15}N$, which is 0.73% in the ambient air [15]. Considering the importance of investigating ^{15}N in the field of environmental science and ecology, the PLF combined Raman spectroscopy can be a good candidate for an *in situ* measurement technique for detecting the abundance of nitrogen isotopes, where mass spectrometry of a sample is currently a standard technique [16].

Additionally, since the PLF technique shares the principal concept with polarization-separation by subtraction, background suppression using these two methods are compared in Fig. 5. Spectral data are from the measurements in the sooting flame, which is discussed more in detail in section 3.3. For the direct subtraction method, subsets of data for vertical and horizontal polarization of the laser were retrieved, averaged, and subtracted. As a result, Raman signal strengths are

Optics EXPRESS

similar for the two methods, but the direct subtraction result presents a higher noise level and larger errors, e.g., negative values. In addition, rotational Raman lines of hydrogen remain with higher intensity at 596, 821, and 1044 cm^{-1}. The quality of the spectrum obtained from direct subtraction is highly dependent on the quality and noise level of selected data sets. On the other hand, the PLF technique shows an advantage in that the filtering process effectively rejects noise and shot-to-shot deviations that occur out of sync with the modulation frequency. However, some residual background signals coupled to the laser modulation, e.g., C_2 emissions, remain, which will be discussed further in section 3.3.

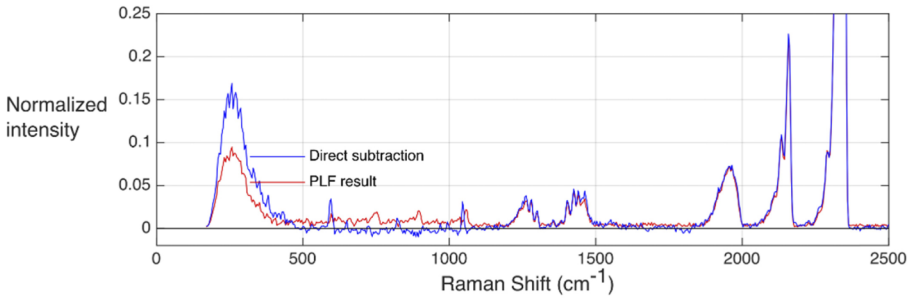

Fig. 5. Comparison between the PLF technique and polarization-separation by direct subtraction. The spectral data are taken from measurements in a sooting flame. Direct subtraction was made for subsets of data acquired with vertical and horizontal polarization of the laser, respectively.

3.2. *Investigations of experimental parameters*

When the absolute strength of Raman signals is important, it is essential to know how the spectrum is affected by the filtering process. Therefore, the effects of some detection setting parameters on the spectra retrieved after the PLF processing were investigated by introducing a controlled fluorescence background to Raman measurements in air.

By utilizing the previously mentioned acetone-seeded airflow, and simultaneous excitation with 266 nm and 532 nm beams, laser-induced fluorescence of acetone was detected together with Raman signals. Before testing the effects of the experimental setting parameters on the Raman spectrum, the filtering quality for different background levels was investigated. The intensity of the 266 nm beam was varied to change the fluorescence background from zero to a level comparable with the Raman signals, and the result is presented in Fig. 6. For this test, the polarization-modulation period was 7 seconds. In addition, data were recorded with 2500 on-chip accumulations, and it continued for the duration of 7 polarization modulation cycles, i.e., 49 seconds. This set of conditions will be referred to as the 'standard setting' in the following.

Panel a) in Fig. 6 shows the data before applying the PLF technique. A broadband background from acetone fluorescence is observed across the entire wavenumber (Raman shift) range. The intensity of the fluorescence is stronger at smaller wavenumbers, and the longpass filter blocking wavelengths shorter than 540 nm suppressed the background at the lowest Raman shifts. Distinct peaks in the data are Raman signals of acetone (782 cm^{-1}), oxygen (1557 cm^{-1}), and nitrogen (2331 cm^{-1}), while two weaker peaks of acetone are located at 1058 and 1737 cm^{-1}. The identification of the acetone peaks (cf., Fig. 6) refers to the previous work by Bradley and Krech [17].

Panel b) shows the absolute intensity of the signal after the PLF processing, where the fluorescence background has been effectively suppressed. Four spectra originally acquired under different background levels overlap each other very well after the filtering, which implies that the PLF worked well for eliminating the fluorescence background for all the investigated levels.

Optics EXPRESS

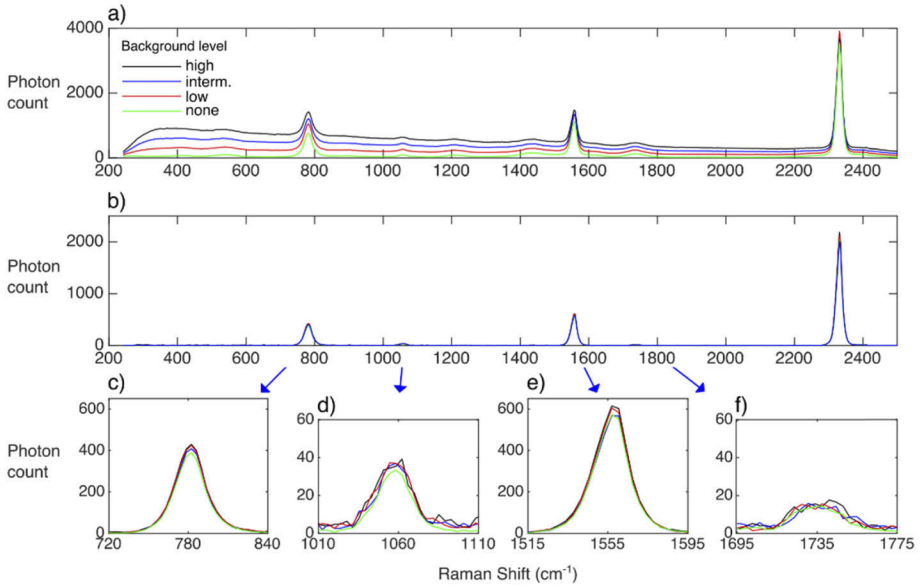

Fig. 6. PLF on Raman spectra of ambient air with acetone fluorescence background. The intensity of the acetone fluorescence has varied from zero to high. a) before applying the PLF, b) after the PLF, c) and d) close-ups of peaks for acetone C-C stretch and C-(C = O)-C breathing motion, e) close-up of oxygen peak, and f) close-up of acetone C = O stretch peak [17].

Panels c) and e) are close-up views of the strong acetone peak and oxygen peak, respectively, and the intensities between the cases vary within 5% of the mean value. The variation in the reconstructed intensity is, possibly, caused by fluctuations of the acetone seeding. The fluctuation can be minimized by normalizing each spectrum to its maximum intensity, i.e., the nitrogen peak, and the results can be compared with each other. Peaks with very weak intensity at 1058 and 1737 cm^{-1}, for which the background is the dominant signal contribution, were also preserved very well through the filtering and became more distinct when free from the background as observed in panel d) and f). The preservation of minor peaks is a great merit of the method for improved detection sensitivity and accuracy since computing the area under these minor peaks for quantification becomes much more accurate by the removal of the background.

The experiments continued with varying the parameters to investigate the preservation of spectral shape and quality under various conditions. Controlled parameters were the period of the polarization modulation, the number of accumulations for one image (recording speed), and the number of images saved (recording duration). From the standard setting, each parameter was changed in turn while keeping the other settings fixed to the standard values. The period of the polarization modulation varied from 3 to 9 seconds with 2 seconds interval where the shortest period was limited by the specification of the rotation mount. The number of accumulations was increased from 1000 to 4000 shots in steps of 500 shots. This parameter is directly affecting the speed of recording, i.e., the frame rate, and 1000 and 4000 accumulations are equivalent to 3.02 and 1.07 frames per second, respectively. The number of images saved was altered to investigate the effect of the modulation phase matching between the first and the last image. Therefore, while 7 cycles of the modulation are equivalent to 49 seconds, the length of the input data was varied from 45 to 53 seconds with an interval of 2 seconds. The variation of the parameters is listed in Table 1.

Optics EXPRESS

Table 1. Setting parameters for the polarization lock-in filtering technique investigated to test the impact on spectral quality. Settings written in bold represent the standard condition.

Controlled Parameters:	Period of Modulation (sec)	Accumulations (# of shots (fps))	Recording Duration (sec)
	3	1000 (3.02)	45
	5	1500 (2.32)	47
	7	2000 (1.88)	**49**
	9	**2500 (1.58)**	51
		3000 (1.37)	53
		3500 (1.20)	
		4000 (1.07)	

Raman spectra of oxygen and nitrogen acquired under the 16 combinations of the conditions are presented in Fig. 7. Different combinations of the parameters affect the absolute intensity of spectra after the Fourier filtering and reconstruction, and therefore, the spectra were normalized to the maximum intensity of the nitrogen signal. As a result, all the spectra show a well-matching shape for baseline level and peak intensities of oxygen and nitrogen Raman signals.

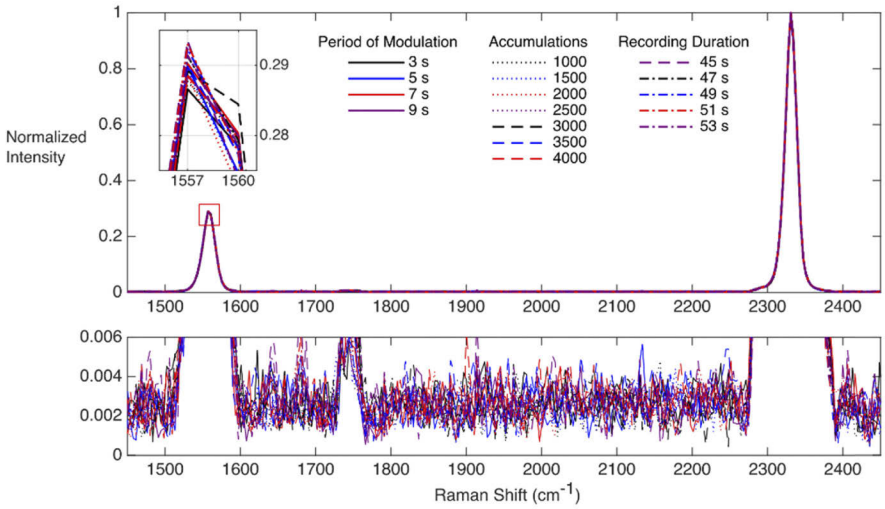

Fig. 7. Raman spectra of air after an acetone fluorescence background has been removed by the PLF method. Raman signals of oxygen and nitrogen at 1557 and 2331 cm^{-1} show good agreement for the 16 different experimental settings investigated. While the standard setting is a modulation period of 7 s, accumulations of 4000 shots, and a recording duration of 49 s, one of these parameters were changed for each case.

The oxygen peak intensities show very good precision with a maximum deviation of 1.3% from their mean value. The baselines at the bottom panel of Fig. 7 are at a similar level, while the deviation from the mean value is minor compared to the noise level of each spectrum. Therefore, it is concluded that the choice of the setting parameters does not affect the quality of the spectrum through the PLF processing. In other words, the PLF method can be applied with the freedom of selecting experimental conditions from slow recording speed with a larger number of accumulations to fast modulation and recording speed, depending on conditions at the measurement volume.

By removing the interfering background, the signal-to-background ratio (SBR) of the spectra has been largely improved. Before the filtering, the ratio of the 782 cm^{-1} acetone peak compared

Optics EXPRESS

to the adjacent background level was between 0.9 and 1.6. After the filtering, signals became much more distinct by removing the background, and it resulted in greatly improved SBRs between 32 and 94. Large variations in the SBRs after the filtering is primarily due to the close-to-zero background level obtained after processing, which has a large impact on the calculated ratio.

3.3. Application of PLF for investigating a sooting flame

In order to test the PLF technique under more challenging and practical background conditions, a sooting flame of ethylene/air at equivalence ratio Φ=2.0 was introduced in the setup. The flame was highly luminous as presented in Fig. 4, and a broadband background signal, primarily from laser-induced incandescence (LII) of soot particles, was covering the Raman signals. The position of the measurement was scanned from 1.5 to 19.5 mm above the burner in 1 mm steps, where the flame stabilizer was located at 21 mm. The results are presented in Fig. 8, where the plot at the top shows raw data before applying the PLF technique, the middle one shows data after the filtering, and the bottom one shows the filtered data with an offset to each spectrum for a better illustration. Some heights were excluded from panel c) due to the large similarity between spectra of adjacent heights.

By comparing the spectra in panels a) and b), it is clearly observed that the LII background level up to 20000 counts was effectively filtered with the PLF technique. Therefore, Raman signals of major combustion species, e.g., carbon dioxide (CO_2), oxygen (O_2), acetylene (C_2H_2), carbon monoxide (CO), nitrogen (N_2), ethylene (C_2H_4), water (H_2O), and hydrogen (H_2), were revealed and are labeled in panel c). Strong signals of supplied reactants, i.e., C_2H_4, O_2, and N_2, were clearly observed at the lowest height, but even products, e.g., H_2 and CO_2, start to appear there. Therefore, it can be expected that a flame front was located at around 1.5 mm above the burner, and this complies with a previous study of similar experimental conditions [18]. At heights above 2.5 mm, only the combustion products and N_2 are detected.

In addition to the Raman peaks, spectra also show residual laser-induced emission peaks of the C_2 Swan bands in the region between 500 and 1000 cm^{-1} that require further discussion for an explanation. For the peak at 1052 cm^{-1}, around 200 out of 2000 counts from the raw data remained after the filtering, even though the C_2 emission signal is unpolarized in general. The appearance of the Swan bands is strongly related to soot sublimation due to the high fluence of the laser utilized in the experiments. The laser fluence in this study was around 60 J/cm^2 at the focus, while it is often set below 0.1 J/cm^2 in soot studies to minimize sublimation [19–21]. The remaining contribution of the Swan bands after the filtering can be explained by the polarization-dependent reflection of the optical components and the resulting laser fluence change. Even though the data were compensated for such effects, sublimation shows a non-linear dependence on laser fluence [22], so a portion of the Swan-band intensity oscillated in phase with the polarization modulation, and thus it remained after the filtering process. If the laser fluence is limited, however, the residue of laser-induced C_2 emission peaks could disappear, and the filtering technique would still be working regardless of the background level.

Spontaneous Raman spectra from sooting flames are rare [6,11,12,23–25], and the spectra at various heights in the flame presented in Fig. 8(c) is already an excellent example of showing how powerful the PLF technique can be. However, straightforward quantification is an important advantage of gas-phase Raman spectroscopy, and therefore, the spectra were converted into a mole fraction plot presented in Fig. 9. The quantification process of Raman spectra consists of calculating the area under each peak in Fig. 8(c) and counting in Raman cross-sections. The integration region for each species is indicated at the bottom of Fig. 8(c). The cross-section values were obtained from the compilation by Eckbreth [13], with a supplement of Gough and Murphy's work for C_2H_2 [26]. Experimental data are presented together with simulation results obtained using the ARAMCO 2.0 kinetic mechanism implemented in the Cantera software

Optics EXPRESS

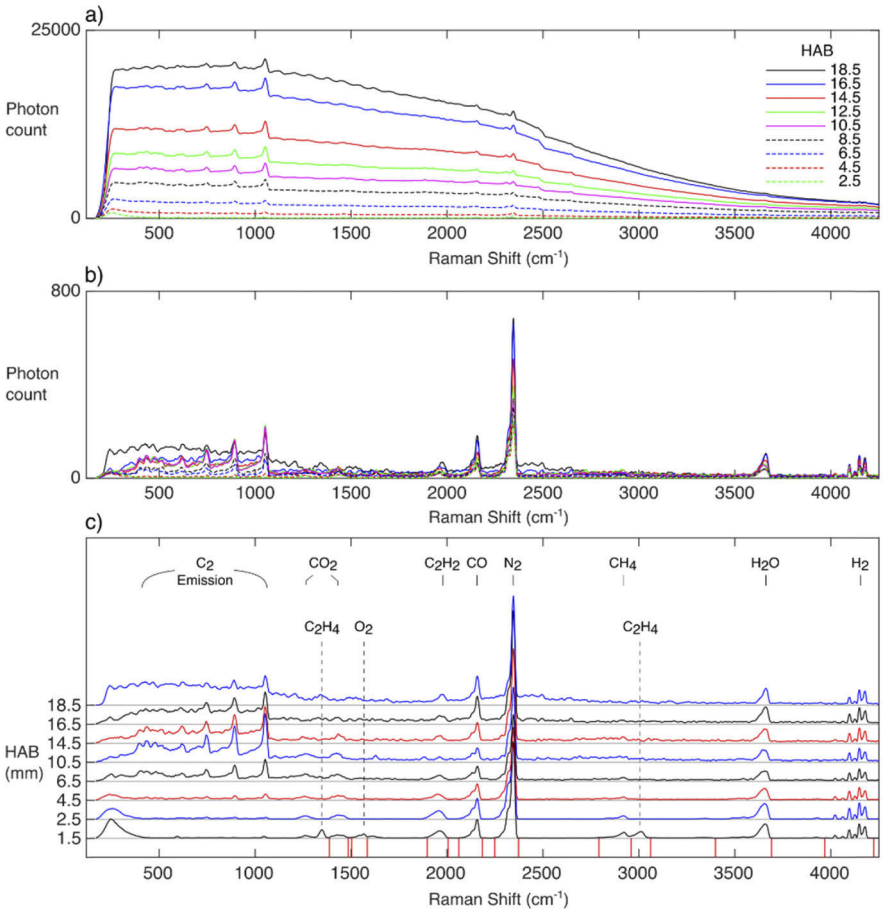

Fig. 8. PLF on Raman spectra of a luminous ethylene/air flame at equivalence ratio Φ=2.0 for various heights above the burner (HAB). a) Spectra before application of PLF show a strong background across the entire wavenumber range. b) Spectra after PLF processing, by which the background has been effectively suppressed. c) Filtered results for some heights plotted with an offset for each HAB for a better illustration. Integration regions for quantitative analyses of species mole fractions are indicated at the Raman-shift axis of panel c).

Optics EXPRESS

with the stagnation plane module [27–34]. The simulation had boundary conditions of an inlet temperature of 298 K and a stagnation plane surface temperature of 900 K at 21 mm HAB.

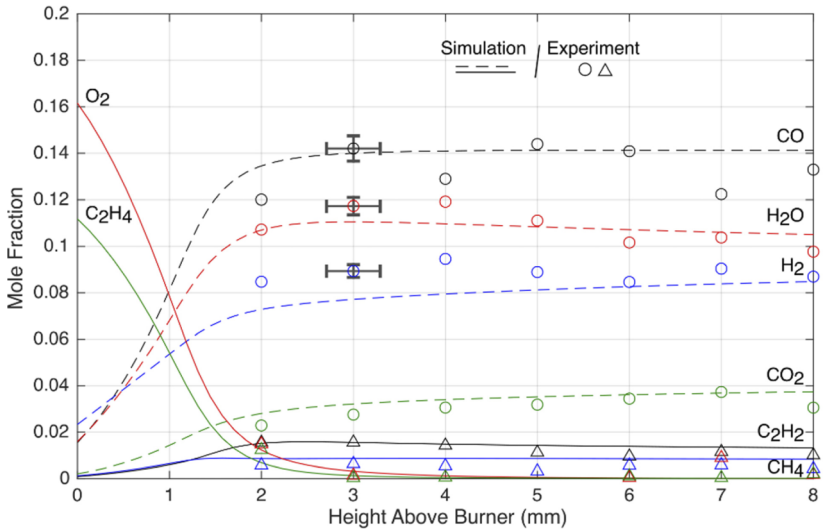

Fig. 9. Mole fractions converted from Raman signals (markers) together with flame simulation results (lines). A 0.5 mm offset in position was added to the experimental data in compliance with the uncertainty estimation. Heights above 8 mm have been excluded due to high noise levels and hence an increase of error. The error bars indicate the range of the largest error estimated from evaluation of the O_2 mole fraction in air and contributions of depolarization ratios (vertical bar), and simulations with 3% variations in inlet conditions (horizontal bar).

The experimental results agree well with the simulation predictions in general. The sublimation was found to add at most 220 ppm of carbon atoms to the flame based on calculations from the soot volume fraction under the given equivalence ratio [35] and has a minor effect on the mole fractions of the species presented in Fig. 9. The hydrogen (H_2) level is overestimated in the experiment, and the error is possibly due to the evaluation of the separated hydrogen Raman peaks that make integration and quantification less accurate. The simulated mole fractions reached plateau levels at heights above 8 mm, but the experimental data showed an increased spread as the height increased. The remaining background level of the filtered spectra for positions above 8 mm was noisier as a result of eliminating a larger background level in the raw data acquired at these positions. In the quantification process, the loss of the Raman signal due to the effect of depolarization was not considered. The maximum error due to the depolarization would be 10% for a depolarization ratio of 0.05; however, all the molecules presented here have lower values than this [36,37]. In addition, some uncertainty could be attributed to crosstalk between spectrally adjacent signals of different species. For example, the overlap between methane and ethylene around 3000 cm^{-1} [cf., Fig. 8(c)]. Detailed investigations on the effect of crosstalk can minimize the error, but in this study, the integration regions for each species were for convenience set at the local minimum between peaks.

Another quantitative analysis available with Raman spectroscopy is gas-phase thermometry using the nitrogen signal. Therefore, spectra were measured for a narrow wavenumber region centered at the nitrogen Q-branch employing the grating with higher resolution in the spectrometer. The PLF-processed data are presented in Fig. 10(a). The vibrational Q-branch Raman signal of nitrogen and its hot bands are clearly observed around 2300 cm^{-1}, which can be utilized for thermometry.

Optics EXPRESS

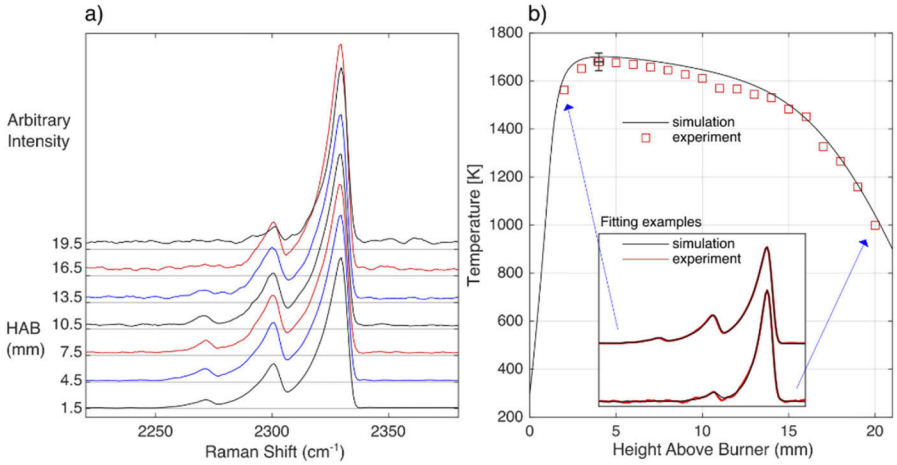

Fig. 10. a) PLF processed spectra of nitrogen in sooting flame plotted with offset values for a better illustration. Fundamental and hot bands of nitrogen are observed. b) Temperature values obtained from the filtered Raman spectra by fitting theoretical spectra in comparison to chemical kinetic simulation results. The insert shows experimental spectra together with the corresponding theoretical spectra obtained by least-squares fitting. A 0.5 mm offset was added to the experimental temperature plot. The error bar indicates the range of the largest error evaluated from the temperature fitting uncertainty and temperature variation in space.

Temperatures at heights between 1.5 mm and 19.5 mm above the burner were evaluated using an in-house developed code. Theoretical spectra simulated with the PGOPHER software [38] were fitted to each experimental spectrum to retrieve the temperature. The values obtained from the spectra at various heights above the burner are presented with square markers in Fig. 10(b). The insert in Fig. 10(b) shows examples of fitted and experimental spectra for the data points indicated by arrows. The maximum temperature of 1680 K from the Raman thermometry is reasonable compared with previous studies under similar flame conditions that reported values between 1680 K and 1790K [39–41]. However, full profiles of temperatures at various heights of the flame for the specific condition of this study are missing. Temperatures obtained from the previously mentioned simulation are also presented in panel (b). An offset of 0.5 mm added to the height values of the experimental data in Fig. 10(a) gives the best overlap between the profiles. The height offset was reasonable considering the uncertainty of the manual adjustment of the burner position and the errors of the mass flow controller units. From simulations under different flow conditions, a change in the mass flow of 3% was found to shift temperature and mole fraction profiles by 0.3 mm in height. Therefore, the height offset was added to the temperatures and also to the mole fraction data in Fig. 9.

The trends of the temperature from the experiment and the simulation agree well, while the predicted temperatures are higher than the measured ones. The maximum difference is 60 K at a height 11 mm above the burner. The temperature differences might be attributed to the formation of soot that was not included in the simulation. The flame of equivalence ratio Φ=2.0 forms rather low amounts of soot (~0.01 ppm in soot volume fraction) [35], so a further discrepancy between simulations and Raman-based thermometry could be expected for even richer flames where a larger amount of soot is formed. However, evaluation of different data sets showed a difference in temperature of ~80 K, as indicated by the error bar in Fig. 10(b). Thus, measurements and model predictions agree within the spread observed for the experimental data sets.

Even with the uncertainties addressed here, the PLF technique made it possible to employ Raman spectroscopy to the sooting flame and retrieve quantitative mole fractions and temperatures

Optics EXPRESS

with realistic values. This strongly confirms that the technique can be very useful for quantitative Raman spectroscopy under challenging experimental conditions. Here, this has been demonstrated for combustion diagnostics, but the concept should be suitable for application in other research where background interferences are the main obstacle that inhibits the application of Raman spectroscopy.

4. Conclusions

In this study, a polarization lock-in filtering (PLF) technique to extend the applicability of Raman spectroscopy by suppressing polarization-independent background signals has been developed and presented. In order to keep the time-resolved information while eliminating the background interferences, the PLF was devised by combining a temporal lock-in filtering method and a polarization-separation concept. The technique is arranged simply by introducing one additional component to the ordinary Raman measurement system. However, the result is efficient suppression of all polarization-independent signals, e.g., fluorescence and black body radiation, while maintaining polarization-dependent signals, e.g., Q-branch vibrational Raman spectra, under continuous measurement.

Firstly, the feasibility of the technique was validated by ambient air measurements, where vibrational Raman signals of nitrogen, oxygen, and carbon dioxide were clearly separated from rotational Raman signals. Secondly, experimental parameters of the PLF technique have been varied for measurements on air with a controlled background from fluorescence in order to understand optimum settings and the limiting factors. The fluorescence background was effectively suppressed for all investigated settings of modulation period, number of accumulations, and recording duration change that has followed, with the quality of spectrum preserved after the filtering. At last, the technique was employed for practical application in a sooting flame accompanied by a strong luminosity and interfering laser-induced background signals. The PLF technique resulted in a 200-fold decrease of the background and allowed for quantitative analyses of mole fractions and temperatures using the filtered spectra.

Since it is a newly introduced technique, naturally, there exist some limitations and room for improvements. For example, it was observed that suppressing larger backgrounds results in a higher noise level of the background in the processed spectra, which can be problematic when directly comparing results under various conditions that originally had different background levels. In addition, while the technique can eliminate polarization-independent terms in a relatively simple way, some more mathematical procedures would be required if the background and Raman signals are not perfectly depolarized and polarized, respectively. Therefore, in this study, fluorescence and luminosity were assumed to be completely depolarized, and Raman signals were not compensated for the intensity loss due to the depolarization. However, it would be possible to compensate for the effects of depolarization ratios and polarized fluorescence in the results by including known parameters on molecular polarizabilities in the data analysis.

While the main application demonstrated in this study was a flame measurement, we believe that the PLF technique can be easily tailored for applications in any field of interest where Raman spectroscopy would be beneficial but is restricted due to background interference.

Funding. Stiftelsen för Strategisk Forskning (ITM17-0313); European Research Council (TUCLA 669466); Energimyndigheten (CECOST 22538-4).

Acknowledgments. We would like to thank Dr. Torsten Methling for developing the program fitting experimental nitrogen Raman spectra for temperature evaluation.

Disclosures. The authors declare no conflicts of interest.

References

1. D. C. Harris and M. D. Bertolucci, *Symmetry and spectroscopy: an introduction to vibrational and electronic spectroscopy* (Courier Corporation, 1989).

Optics EXPRESS

2. E. Kristensson, J. Bood, M. Aldén, E. Nordstrom, J. Zhu, S. Huldt, P. E. Bengtsson, H. Nilsson, E. Berrocal, and A. Ehn, "Stray light suppression in spectroscopy using periodic shadowing," Opt. Express **22**(7), 7711–7721 (2014).
3. D. Wei, S. Chen, and Q. Liu, "Review of Fluorescence Suppression Techniques in Raman Spectroscopy," Appl. Spectrosc. Rev. **50**(5), 387–406 (2015).
4. A. C. De Luca, K. Dholakia, and M. Mazilu, "Modulated Raman spectroscopy for enhanced cancer diagnosis at the cellular level," Sensors **15**(6), 13680–13704 (2015).
5. C. A. Arguello, G. F. Mendes, and R. C. Leite, "Simple technique to suppress spurious luminescence in Raman spectroscopy," Appl. Opt. **13**(8), 1731–1732 (1974).
6. J. Egermann, T. Seeger, and A. Leipertz, "Application of 266-nm and 355-nm Nd:YAG laser radiation for the investigation of fuel-rich sooting hydrocarbon flames by Raman scattering," Appl. Opt. **43**(29), 5564–5574 (2004).
7. J. J. Kojima and D. G. Fischer, "Multiscalar Analyses of High-Pressure Swirl-Stabilized Combustion Via Single-Shot Dual-Sbg Raman Spectroscopy," Combust. Sci. Technol. **185**(12), 1735–1761 (2013).
8. A. Luczak, V. Beushausen, S. Eisenberg, M. Knapp, H. Schluter, P. Andresen, M. Malobabic, and A. Schmidt, "New nonintrusive laser diagnostic tools for design and optimization of technically applied combustion systems," Combust. Sci. Technol. **116-117**(1-6), 541–566 (1996).
9. F. Rabenstein and A. Leipertz, "One-dimensional, time-resolved Raman measurements in a sooting flame made with 355-nm excitation," Appl. Opt. **37**(21), 4937–4943 (1998).
10. G. Grünefeld, V. Beushausen, P. Andresen, and W. Hentschel, "Spatially resolved Raman scattering for multi-species and temperature analysis in technically applied combustion systems: spray flame and four-cylinder in-line engine," Appl. Phys. B **58**(4), 333–342 (1994).
11. J. Kojima, D. Fischer, and Q.-V. Nguyen, "Subframe burst gating for Raman spectroscopy in combustion," Opt. Lett. **35**(9), 1323–1325 (2010).
12. G. Magnotti, D. Geyer, and R. S. Barlow, "Interference free spontaneous Raman spectroscopy for measurements in rich hydrocarbon flames," Proc. Combust. Inst. **35**(3), 3765–3772 (2015).
13. A. C. Eckbreth, *Laser diagnostics for combustion temperature and species* (CRC press, 1996), Vol. 3.
14. D. A. Long, *Raman spectroscopy* (Mcgraw-Hill, 1977).
15. G. Junk and H. J. Svec, "The Absolute Abundance of the Nitrogen Isotopes in the Atmosphere and Compressed Gas from Various Sources," Geochim. Cosmochim. Acta **14**(3), 234–243 (1958).
16. P. A. De Groot, *Handbook of stable isotope analytical techniques* (Elsevier, 2004), Vol. 1.
17. M. S. Bradley and J. H. Krech, "High-pressure Raman spectra of the acetone carbon-carbon stretch in binary liquid mixtures with methanol," J. Phys. Chem. **96**(1), 75–79 (1992).
18. C. Brackmann, J. Bood, P. E. Bengtsson, T. Seeger, M. Schenk, and A. Leipertz, "Simultaneous vibrational and pure rotational coherent anti-stokes Raman spectroscopy for temperature and multispecies concentration measurements demonstrated in sooting flames," Appl. Opt. **41**(3), 564–572 (2002).
19. H. A. Michelsen, "Understanding and predicting the temporal response of laser-induced incandescence from carbonaceous particles," J. Chem. Phys. **118**(15), 7012–7045 (2003).
20. N. E. Olofsson, J. Simonsson, S. Torok, H. Bladh, and P. E. Bengtsson, "Evolution of properties for aging soot in premixed flat flames studied by laser-induced incandescence and elastic light scattering," Appl. Phys. B **119**(4), 669–683 (2015).
21. F. Goulay, L. Nemes, P. E. Schrader, and H. A. Michelsen, "Spontaneous emission from C_2 ($d\ ^3\Pi_g$) and C_3 ($A\ ^1\Pi_u$) during laser irradiation of soot particles," Mol. Phys. **108**(7-9), 1013–1025 (2010).
22. P.-E. Bengtsson and M. Aldén, "Optical investigation of laser-produced C_2 in premixed sooty ethylene flames," Combust. Flame **80**(3-4), 322–328 (1990).
23. G. Grünefeld, V. Beushausen, and P. Andresen, "Interference-free UV-laser-induced Raman and Rayleigh measurements in hydrocarbon combustion using polarization properties," Appl. Phys. B **61**(5), 473–478 (1995).
24. W. Meier and O. Keck, "Laser Raman scattering in fuel-rich flames: Background levels at different excitation wavelengths," Meas. Sci. Technol. **13**(5), 741–749 (2002).
25. C. Yang, H. Tang, and G. Magnotti, "Picosecond Kerr-gated Raman spectroscopy for measurements in sooty and PAH rich hydrocarbon flames," *Proc. Combust. Inst.* (2020).
26. K. M. Gough and W. F. Murphy, "The Raman-Scattering Intensity Parameters of Acetylene," J. Mol. Struct. **224**, 73–88 (1990).
27. A. Kéromnès, W. K. Metcalfe, K. A. Heufer, N. Donohoe, A. K. Das, C.-J. Sung, J. Herzler, C. Naumann, P. Griebel, and O. Mathieu, "An experimental and detailed chemical kinetic modeling study of hydrogen and syngas mixture oxidation at elevated pressures," Combust. Flame **160**(6), 995–1011 (2013).
28. W. K. Metcalfe, S. M. Burke, S. S. Ahmed, and H. J. Curran, "A hierarchical and comparative kinetic modeling study of $C_1 - C_2$ hydrocarbon and oxygenated fuels," Int. J. Chem. Kinet. **45**(10), 638–675 (2013).
29. S. M. Burke, W. Metcalfe, O. Herbinet, F. Battin-Leclerc, F. M. Haas, J. Santner, F. L. Dryer, and H. J. Curran, "An experimental and modeling study of propene oxidation. Part 1: Speciation measurements in jet-stirred and flow reactors," Combust. Flame **161**(11), 2765–2784 (2014).
30. S. M. Burke, U. Burke, R. Mc Donagh, O. Mathieu, I. Osorio, C. Keesee, A. Morones, E. L. Petersen, W. J. Wang, T. A. DeVerter, M. A. Oehlschlaeger, B. Rhodes, R. K. Hanson, D. F. Davidson, B. W. Weber, C. J. Sung, J. Santner, Y. G. Ju, F. M. Haas, F. L. Dryer, E. N. Volkov, E. J. K. Nilsson, A. A. Konnov, M. Alrefae, F. Khaled, A. Farooq, P.

Optics EXPRESS

Dirrenberger, P. A. Glaude, F. Battin-Leclerc, and H. J. Curran, "An experimental and modeling study of propene oxidation. Part 2: Ignition delay time and flame speed measurements," Combust. Flame **162**(2), 296–314 (2015).
31. U. Burke, W. K. Metcalfe, S. M. Burke, K. A. Heufer, P. Dagaut, and H. J. Curran, "A detailed chemical kinetic modeling, ignition delay time and jet-stirred reactor study of methanol oxidation," Combust. Flame **165**, 125–136 (2016).
32. C. W. Zhou, Y. Li, E. O'Connor, K. P. Somers, S. Thion, C. Keesee, O. Mathieu, E. L. Petersen, T. A. DeVerter, M. A. Oehlschlaeger, G. Kukkadapu, C. J. Sung, M. Alrefae, F. Khaled, A. Farooq, P. Dirrenberger, P. A. Glaude, F. Battin-Leclerc, J. Santner, Y. G. Ju, T. Held, F. M. Haas, F. L. Dryer, and H. J. Curran, "A comprehensive experimental and modeling study of isobutene oxidation," Combust. Flame **167**, 353–379 (2016).
33. Y. Li, C. W. Zhou, K. P. Somers, K. W. Zhang, and H. J. Curran, "The oxidation of 2-butene: A high pressure ignition delay, kinetic modeling study and reactivity comparison with isobutene and 1-butene," Proc. Combust. Inst. **36**(1), 403–411 (2017).
34. D. G. Goodwin, R. L. Speth, H. K. Moffat, and B. W. Weber, "Cantera: An object-oriented software toolkit for chemical kinetics, thermodynamics, and transport processes," https://www.cantera.org, 2018. (Version 2.4.0).
35. R. Hadef, K. P. Geigle, W. Meier, and M. Aigner, "Soot characterization with laser-induced incandescence applied to a laminar premixed ethylene-air flame," Int. J. Therm. Sci. **49**(8), 1457–1467 (2010).
36. F. Baas and K. Van den Hout, "Measurements of depolarization ratios and polarizability anisotropies of gaseous molecules," Phys. A **95**(3), 597–601 (1979).
37. S. Danichkin, A. Eliseev, T. Popova, O. Ravodina, and V. Stenina, "Raman scattering parameters for gas molecules (survey)," J. Appl. Spectrosc. **35**(4), 1057–1066 (1981).
38. C. M. Western, "PGOPHER: A program for simulating rotational, vibrational and electronic spectra," J. Quant. Spectrosc. Radiat. Transfer **186**, 221–242 (2017).
39. F. Vestin, M. Afzelius, C. Brackmann, and P. E. Bengtsson, "Dual-broadband rotational CARS thermometry in the product gas of hydrocarbon flames," Proc. Combust. Inst. **30**(1), 1673–1680 (2005).
40. B. Zhao, Z. W. Yang, Z. G. Li, M. V. Johnston, and H. Wang, "Particle size distribution function of incipient soot in laminar premixed ethylene flames: effect of flame temperature," Proc. Combust. Inst. **30**(1), 1441–1448 (2005).
41. Q. Wu, F. Wang, M. Y. Li, J. H. Yan, and K. F. Cen, "Simultaneous In-Situ Measurement of Soot Volume Fraction, H_2O Concentration, and Temperature in an Ethylene/Air Premixed Flame Using Tunable Diode Laser Absorption Spectroscopy," Combust. Sci. Technol. **189**(9), 1571–1590 (2017).